Title: Effectiveness of Create ML in microscopy image classifications: A simple and inexpensive deep learning pipeline for non-data scientists

Short title: A simple and inexpensive deep learning pipeline for non-data scientists

Author names: Kiyotaka Nagaki[1], Tomoyuki Furuta[1], Naoki Yamaji[1], Daichi Kuniyoshi[2], Megumi Ishihara[2], Yuji Kishima[2], Minoru Murata[3], Atsushi Hoshino[4, 5] and Hirotomo Takatsuka[6, 7]

Affiliations of the authors:

1. Institute of Plant Science and Resources, Okayama University, Kurashiki 710-0046, Japan

2. Laboratory of Plant Breeding, Research Faculty of Agriculture, Hokkaido University, Sapporo 060-8589, Japan

3. Department of Agricultural and Food Science, Universiti Tunku Abdul Rahman, Kampar, Perak 31900, Malaysia

4. National Institute for Basic Biology, Okazaki 444-8585, Japan

5. Department of Basic Biology, SOKENDAI (The Graduate University for Advanced Studies), Okazaki 444-8585, Japan

6. Graduate School of Science and Technology, Nara Institute of Science and Technology, 8916-5 Takayama,

Ikoma, Nara 630-0192, Japan

7. Present address: School of Biological Science and Technology, College of Science and Engineering, Kanazawa University, Kakuma-machi, Kanazawa, 920-1192 Japan

Communicating author: Kiyotaka Nagaki

E-mail: nagaki@rib.okayama-u.ac.jp

Tel: +81-86-434-1208

Fax: +81-86-434-1208

Abstract

Observing chromosomes is a time-consuming and labor-intensive process, and chromosomes have been analyzed manually for many years. In the last decade, automated acquisition systems for microscopic images have advanced dramatically due to advances in their controlling computer systems, and nowadays it is possible to automatically acquire sets of tiling-images consisting of large number, more than 1,000, of images from large areas of specimens. However, there has been no simple and inexpensive system to efficiently select images containing mitotic cells among these images. In this paper, a classification system of chromosomal images by deep learning artificial intelligence (AI) that can be easily handled by non-data scientists was applied. With this system, models suitable for our own samples could be easily built on a Macintosh computer with Create ML. As examples, models constructed by learning using chromosome images derived from various plant species were able to classify images containing mitotic cells among samples from plant species not used for learning in addition to samples from the species used. The system also worked for cells in tissue sections and tetrads. Since this system is inexpensive and can be easily trained via deep learning using scientists' own samples, it can be used not only for chromosomal image analysis but also for analysis of other biology-related images.

Keywords

Machine learning, deep learning, mitotic cell, chromosome, tetrad, microscope

Declarations

Funding:

This work was partly supported by grants from JSPS KAKENHI (No. 19H00937 to Yuji Kishima), the Joint Usage/Research Center, Institute of Plant Science and Resources, Okayama University (Nos. 2838 to Hirotomo Takatsuka, 2839 to Atsushi Hoshino, R240 to Yuji Kishima and IP2019 to Minoru Murata), and the NIBB Collaborative Research Program (20-328 to Atsushi Hoshino).

Conflicts of interest/Competing interests:

The authors have no relevant financial or non-financial interests to disclose. The authors have no conflicts of interest to declare that are relevant to the content of this article. All authors certify that they have no affiliations with or involvement in any organization or entity with any financial interest or non-financial interest in the subject matter or materials discussed in this manuscript. The authors have no financial or proprietary interests in any material discussed in this article. Authors are responsible for correctness of the statements provided in the manuscript. See also Authorship Principles. The Editor-in-Chief reserves the

right to reject submissions that do not meet the guidelines described in this section.

Availability of data and material:

The datasets generated during and/or analyzed during the current study are available from the corresponding author on reasonable request.

Code availability:

CutSort is freely available on GitHub (https://github.com/tomoyukif/CutSort).

Authors' contributions:

Kiyotaka Nagaki conceived the study; conducted the experiments except the CLSM imaging and the preparation and capture of the *I. nil*, *A. thaliana*, *E. guineensis* and *S. weddelliana* chromosome images and tetrad images; performed the deep learning; produced all the figures; and wrote the manuscript. Tomoyuki Furuta developed the sorting application and reviewed the manuscript. Naoki Yamaji conducted the CLSM imaging. Daichi Kuniyoshi, Megumi Ishihara and Yuji Kishima conducted the tetrad analysis. Atsushi Hoshino (*I. nil*), Hirotomo Takatsuka (*A. thaliana*) and Minoru Murata (*E. guineensis* and *S. weddelliana*)

prepared and captured the chromosome images.

Acknowledgments

I. nil seeds were provided by the National BioResource Project (NBRP). The seeds of *N. tabacum*, *N. sylvestris*, and *N. tomentosiformis* were gifts from Japan Tobacco, Inc. The stems of *S. officinarum* were gifts from the Japan International Research Center for Agricultural Sciences.

Abbreviations

Asa: *Allium sativum*

Ace: *Allium cepa*

Afi: *Allium fistulosum*

AI: artificial intelligence

At: *Arabidopsis thaliana*

Asa: *Allium sativum*

AtCell: *Arabidopsis thaliana* cultured cell

Atu: *Allium tuberosum*

BY-2: *Nicotiana tabacum* cultured cell line BY-2

CLI: Command line interface

Eg: *Elaeis guineensis*

GUI: Graphical user interface

Ha: *Helianthus annuus*

IC: Image classifier

IC (+op): Image classifier with options

Ini: *Ipomoea nil*

Je: *Juncus effusus*

Ln: *Luzula nivea*

Mw: *Microcoelum weddelliana*

Ns: *Nicotiana sylvestris*

Nt: *Nicotiana tabacum*

Nto: *Nicotiana tomentosiformis*

OD: Object detector

Os: *Oryza sativa*

OsCell: *Oryza sativa* cultured cell

PNG: Portable network graphics

So: *Saccharum officinarum*

Ta: *Triticum aestivum*

Introduction

Cell division is the basic process underlying cell proliferation. Chromosomes observed during metaphase of cell division have also been used for karyotype analysis and have played an important role in taxonomy and medicine (Sears 1969; Mandáková and Lysak 2008; Ferguson-Smith and Trifonov 2007; O'Connor 2008). Since Waldeyer's discovery of cell division and chromosomes, cytogeneticists have manually observed, captured and analyzed them for a long time (Waldeyer 1888; Cremer and Cremer 1988). In recent years, both the automation of microscopes and their speed have advanced, and it has become possible to acquire many images in a short time; however, the automation of cytogenetic analysis is limited to some species and applications (Hernández-Mier et al. 2020; Abid et al. 2017; Munot et al. 2011; Shirley et al. 2017). Many analytical applications are optimized for medical purposes, which are important and well-funded applications but often are not applicable in species other than humans and laboratory animals. Plants have very large genomic size variations and therefore have a wide variety of chromosome numbers and sizes (Pellicer and Leitch 2020). Due to this diversity, it is difficult to utilize these analytical applications in plant cytogenetics. In addition, the research field is less funded than the medical field is, making it difficult to develop specialized applications.

Recently, as more flexible applications, approaches using machine learning (including deep learning),

128 have been used for chromosome and cell analysis (LI et al. 2016; Kutsuna et al. 2012; Xiao et al. 2020; Du
129 et al. 2011; Al-Kofahi et al. 2018; McQuin et al. 2018; Shimahara et al. 2019). In these analyses, one's
130 own images can be used as training data such that it is possible to analyze various images. For example,
131 deep learning artificial intelligence (AI) makes it possible to detect individual cells and metaphase
132 chromosomes and to detect and classify cells at each stage of cell division (Kutsuna et al. 2012; Du et al.
133 2011). However, these deep learning pipelines require computing skills need to handle data and tools via
134 command line interfaces (CLIs), which pose a major barrier to non-data scientists such as general
135 cytogeneticists. There are various levels of difficulty associated with these pipelines, from those that handle
136 everything related to the CLI to those involving the addition of plugins to graphical user interface (GUI)
137 applications using the CLI. Even in the simplest example using a free analysis application (CellProfiler),
138 the application has a plug-in for deep learning, and unfortunately, users have to manually install the plug-
139 in via the CLI, which may be a task beyond the computation skills of non-data scientists (McQuin et al.
140 2018). As alternative choices for those who are unfamiliar with CLIs, several companies sell GUI-based
141 applications that provide deep learning pipelines. Even though these applications enable us to apply cutting-
142 edge technologies such as AI-based image processing with a user-friendly interface, they are expensive
143 [LPIXEL's IMACEL (Shimahara et al. 2019), Nikon's NIS.ai, Olympus's TruAI, and Zeiss's ZEN

Intellesis, etc.].

In recent years, deep learning of images has begun to be used not only in the scientific field but also in various other fields, such as facial recognition and object detection for automatic driving. Along with this development, tools for creating personal models for image classification and object detection using proprietary image data have also been developed [Caffe (Jia et al. 2014), TensorFlow (Abadi et al. 2015), AutoML by Google (https://cloud.google.com/automl), Create ML by Apple (https://developer.apple.com/machine-learning/create-ml/)]. Among them, Apple's Create ML is a freely available GUI-based application providing a deep learning framework. Create ML enables users to build one's own model with a highly user-friendly interface. Unfortunately, this application currently offers only one predefined neural network for each category of tasks, e.g., sound recognition, image classification, and object detection. Even though this limitation makes Create ML inflexible for modifying a network structure to improve model performance, this application is attractive for non-data scientists who are willing to utilize deep learning, even in wet labs.

In this paper, we evaluated the performance of deep learning models for image classification and object detection created via Create ML using cytogenetic images as learning data. We assumed that we automatically obtained tiled images from a large tissue section containing some number of cells that should

be classified into categories based on cell types to conduct downstream analyses. The models were built to detect images or positions in images containing cells undergoing cell division. The detection accuracy of the models was measured using test datasets based on the number of cells correctly classified. Our deep learning pipeline consisting of Create ML and support applications enables cytogeneticists to apply deep learning techniques using only GUI-based interfaces.

Materials and methods

Plant materials and plant cell lines

Seeds of *Allium fistulosum* (2*n*=2*x*=16), *Allium tuberosum* (2*n*=4*x*=32), *Arabidopsis thaliana* (2*n*=2*x*=10), *Nicotiana tabacum* cv. SR1 (2*n*=4*x*=48), *Nicotiana sylvestris* (2*n*=2*x*=24), *Nicotiana tomentosiformis* (2*n*=2*x*=24), *Luzula nivea* (2*n*=12), *Oryza sativa* cv. Nipponbare (2*n*=2*x*=24), *Triticum aestivum* cv. Chinese Spring (2*n*=6*x*=42), *Ipomoea nil* cv. Tokyo Kokei Standard (2*n*=2*x*=30), *Helianthus annuus* (2*n*=2*x*=34), and *Juncus effusus* (2*n*=2*x* =40) were germinated on moistened filter paper at room temperature, and stems of *Saccharum officinarum* cv. Ogasawara (2*n*=80) were also grown under the same conditions. Bulbs of *Allium cepa* (2*n*=2*x*=16) and *Allium sativum* (2*n*=2*x*=16) were cultivated by hydroponic culture, and *Elaeis guineensis* (2*n*=2*x*=32) and *Syagrus weddelliana* (2*n*=2*x*=32) plants were

obtained from commercial sources and grown in a greenhouse.

Tobacco cultured cells, BY-2 (Kato et al. 1972), were used in this study. The BY-2 cells were maintained in modified Murashige and Skoog (MS) media consisting of 2.5 mM KH_2PO_4, 3 mM thiamine HCl, 3% (w/v) sucrose, and 1 μM 2,4-dichlorophenoxyacetic acid (2,4-D) on a rotary shaker at 22°C in the dark.

Cultured cells were obtained from seedlings of *A. thaliana*, (L.) Heynh ecotype Columbia (Col-0) (Nagaki et al. 2010). The cells were cultured in MS media consisting of B5 vitamin and 4.5 μM 2,4-D on a rotary shaker at 22°C in the dark.

Capturing images of cells

Root tips and cultured cells were fixed in methanol:glacial acetic acid (3:1). For *A. cepa*, *A. sativum, A. fistulosum*, *A. tuberosum* and *T. aestivum,* cells of the root tips were squeezed and compressed in 45% (v/v) acetic acid on slide glasses. For the other species, the fixed root tips and cultured cells were washed and digested with a mixture of 1% (w/v) cellulase Onozuka RS (Yakult Pharmaceutical Industry, Tokyo, Japan) and 0.5% (w/v) pectolyase Y-23 (Seishin Pharmaceuticals, Tokyo, Japan) and then compressed on glass slides. Chromosomes and nuclei were counterstained with 0.1 μg/ml 4,6-diamino-2-phenylindole (DAPI). The stained chromosomes and nuclei were captured using a chilled charge-coupled device (CCD) camera, AxioCam HR (Carl Zeiss, Oberkochen, Germany) and AxioVision software (Carl Zeiss). For tile capture, stained chromosomes and nuclei were captured by a fluorescence microscope (BZ-9000; Keyence, Osaka, Japan) using image-capturing software built into the BZ-9000 system.

Immunohistochemical analysis of root slices

Immunohistochemical staining was conducted as described by Nagaki et al. (2012), with minor modifications. Two-day-old roots from bulbs of *A. sativum* grown under hydroponic culture were fixed in solutions of microtubule-stabilizing buffer [5 mM PIPES (pH 6.9), 0.5 mM MgSO4, and 0.5 mM EGTA] consisting of 3% (w/v) paraformaldehyde (PFA) and 0.3% (v/v) Triton X-100. After fixation, the tissues were washed twice in phosphate-buffered saline (PBS) for 10 min at room temperature. The washed roots were directly glued to the stage of a microslicer (LinearSlicer PRO10; Dosaka EM, Kyoto, Japan) with instant adhesive and then sectioned at a thickness of 100 μm. These sections were transferred onto slide glasses and then macerated in a solution of 0.1% (w/v) pectolyase Y-23 and 0.3% (w/v) Triton X-100 in PBS at room temperature. The macerated slices were subsequently washed three times in PBS, and the primary antibody solutions consisted of 1:100 diluted primary antibody solutions in a blocking solution [100 mM Tris-HCl, 150 mM NaCl and 0.5% (w/v) blocking reagent (Sigma-Aldrich, St. Louis, MO, USA)]. Anti-AfiCENH3 rabbit antibodies (Nagaki et al. 2012) for centromere-specific histone H3 variant (CENH3) and monoclonal anti-α-tubulin antibodies produced in mice (T6199, Sigma-Aldrich) were applied to the slides. The samples were then kept at 4°C for 12-16 h and washed twice in PBS for 10 min at room temperature. After washing in PBS, the secondary antibodies used were Alexa Fluor 555-labeled anti-rabbit antibodies (Molecular Probes, Eugene, OR, USA) and Alexa Fluor 488-labeled anti-mouse antibodies (Molecular Probes). Both antibodies were diluted to 1:500 with blocking solution, reacted at 37°C for 1 h and then washed in the same manner as the primary antibodies were. Chromosomes and nuclei were counterstained with 0.1 μg/ml DAPI and washed in the same manner as the primary antibodies were. After washing, the tissues were mounted with the antifade agent SlowFade (Thermo Fisher Scientific, Waltham,

MA, USA). Confocal analyses were performed on a Leica TCS SP8x (Leica Microsystems, Wetzlar, Germany) equipped with a 405 nm diode laser and a white-light laser (WLL). The excitation and detection wavelengths (nm) were as follows: for DAPI, 405 and 440-460; for Alexa Fluor 488, 500 and 508-525; and for Alexa Fluor 555, 555 and 562-580. To avoid crosstalk between fluorescence dyes, sequential scanning between the 405 nm diode laser and WLL and time gate detection for WLL excitation were used.

Analysis of tetrads

A tetraploid rice line (*O. sativ*a ssp. Indica cv. PUSUR-4x) was provided by the Genebank Project, National Agriculture and Food Research Organization. Isolation of pollen mother cells (PMCs) and preparations for microscopic observations were performed based on the method described by Kuniyoshi et al. (2020), with minor modifications. To obtain anthers containing PMCs at the tetrad stage, panicles were collected at the booting stage when the distance between the auricle of the flag leaf and penultimate leaf was -3 to 0 cm. These panicles were fixed with microtubule-stabilizing buffer consisting of 3% (w/v) PFA and 0.1% (v/v) Triton X-100. The PMCs in the anthers were taken from the spikelets, immersed in 20 µl of 1× PBS and then frozen. The samples were subsequently treated with the primary antibody solutions containing the anti-α-tubulin mouse antibodies, kept at 37°C for 1 h. After the primary reaction occurred, the samples were rinsed with 1× PBS for 10 min. The secondary antibody solutions containing an Alexa Fluor 488-labeled anti-mouse antibody solution were then applied. After incubation at 37°C for 1 h, the samples were rinsed three times with 1× PBS and mounted in 20 µl of ProLong Diamond Antifade with DAPI (Thermo Fisher Scientific) to stain the DNA of the samples.

Deep learning model construction and image classification

An overview of the evaluation workflow for image classification and object detection using Create ML is shown in **Fig. 1**. For the classification of images containing dividing chromosomes and nuclei, learning was performed using images in portable network graphics (PNG) format (1,300 × 1,030 pixels) captured with a Zeiss microscope, image classifier in Create ML [a developer tool of X-code version 11.3, Apple (Cupertino, CA, USA), https://developer.apple.com/download/more/] and a MacBook Air (Apple, Retina, 13-inch, 2019, with a 1.6 GHz dual-core Intel Core i5 CPU, an Intel UHD Graphics 617 GPU and 16 Gb of memory). In the cases of the image classifier, learning was performed with and without augmentation options ("Add Noise", "Blur", "Expose", "Flip" and "Rotate"). For object detection in images containing dividing chromosomes, the same images were used for the image classification and for the object detector in Create ML, and the same computer was used, with an external GPU [Radeon RX 590, Advanced Micro Devices (AMD), Sunnyvale, CA, USA]. In the cases of object detection, when dividing cell(s) were detected in the image, the image was classified as "Chromosomes".

For object detection in immunohistochemistry images, learning was performed using images in PNG format captured with a Leica microscope and the same computer system that was used for object detection. Objects in the images were annotated using RectLabel version 3.04.3 (https://rectlabel.com), and jason files were exported by the application. The images and jason files were used for creation of models via the object detector mode in Create ML. The application can also leverage the model created by Create ML to classify multiple images and annotate objects in those images. The classified images were sorted into folders by an image sorter (CutSort) developed in this study as a support tool. CutSort is freely available on GitHub (https://github.com/tomoyukif/CutSort).

For object detection in images of the tetrads, learning was performed using images in PNG format captured with the Keyence microscope and a MacPro (Apple, 2019 with a 3.5 GHz 8-core Intel Xeon W

CPU, an AMD Radeon Pro W5500X GPU and 32 Gb of memory). Annotations of objects for learning, creation of the model and annotations of objects by AI using the constructed model were conducted by the MacPro machine using the same applications as those used for object detection in the immunohistochemistry images.

Data availability

The models created in this study can be downloaded from GuiHub (https://github.com/tomoyukif/nagakiCreateMLmodels).

Results

Image classification for sorting microscopy images containing mitotic cells

As the first example, classification of images into two classes ("Chromosomes", which includes images showing cells undergoing mitosis, from prometaphase to telophase, and "Others", which include images without cells undergoing mitosis) from captured chromosomal specimen images was attempted (**Fig. S1**). If this classification is possible, automatic selection of images containing mitotic cells from the automatically captured images is possible. In the case of plant-derived samples, the frequency of cells in mitosis is lower than those of cultured animal cells because they cannot be highly synchronized. For this reason, it is necessary to observe a large number of cells in order to find mitotic cells, and this automation

279 is very useful for this purpose. For learning the classification, images containing root cells from nine plant
280 species and three cultured cells were used (**Table S1**). The models built from those learning methods were
281 validated by a validation dataset. In the validation dataset, in addition to the images of the species and cell
282 types used for learning, cell images derived from eight nontrained species were also used (**Table S1**).
283 Initially, three different sized datasets (Mix-60 [a data set consisting of 60 images from multiple species],
284 Mix-120 [a data set consisting of 120 images from multiple species] and Mix-767 [a data set consisting of
285 767 images from multiple species]) were tested to determine how much data were needed to obtain valid
286 models using the system. The learning dataset Mix-60 includes five images with mitotic cells from the 12
287 samples and 15 images without mitotic cells from four samples (**Table S1**) and was used for deep learning
288 with iteration numbers automatically indicated by Create ML. For the construction of models, the image
289 classifier without the options (IC), the image classifier with the options [IC (+op)] and the object detector
290 (OD) took 28 s, 1 h 44 min and 1 h 18 min, respectively (**Table S2**). As a result, the models created by IC,
291 IC (+op) and OD using Mix-60 were 83%, 82% and 91% accurate in the validations, respectively (**Fig. 2**).
292 These models also selected images containing mitotic cells with 40-100% accuracy from images derived
293 from species and cells not used for training (**Fig. S2**). In detail, the accuracy of the classification of small
294 chromosomes tends to be lower for the IC and IC (+op), whereas they tend to be higher for the OD (**Fig.**

295 **S2** and **Table S3**).

296 The relatively large learning dataset (Mix-120) and the largest learning dataset (Mix-767) include ten
297 images with mitotic cells from the 12 samples and 30 images without mitotic cells from four samples and
298 include 767 images with mitotic cells from the 12 samples and 232 images without mitotic cells from four
299 samples, respectively (**Table S1**). These datasets were used for deep learning and image classification. As
300 a result, the models created by IC and OD via Mix-120 and Mix-767 showed much higher accuracies than
301 did those via Mix-60 in the validations (**Fig. 2**). In detail, they showed trends similar to those of the case of
302 Mix-60 but with improved overall accuracy (**Fig. S2**). However, the options of IC were not effective, and
303 the accuracies of IC (+OP) in both were almost the same as those of Mix-60 in the validations (**Fig. 2**).
304 Since the difference in accuracy between the models trained with Mix-120 and Mix-767 is small, these
305 results suggest that if 120 images are prepared per class, mitotic cell image classification models with more
306 than 80% accuracy can be obtained by these methods.

307 The importance of image diversity was then examined by comparing three independent learning datasets
308 consisting of 120 images containing mitotic cells from species or a cultured cell with medium-sized
309 chromosomes (Nt-120, BY-2-120, and Ha-120) and Mix-120, which contains images from nine species and
310 three cultured cell lines (**Tables S2** and **S3**). As a result, the models created by IC, IC (+op) and OD using

311 those learning datasets showed lower accuracy (55-78%) than did those (82-97%) of the mixed learning
312 dataset (Mix-120) in the validations (**Fig. 2**). In detail, the accuracies in the large- and small-chromosome
313 species were quite low (**Fig. S2** and **Table S3**) because those input samples had medium-sized
314 chromosomes. Except for images derived from the species having a chromosome size similar to that of the
315 species used in the learning dataset, the results show that 120 images from a single sample have relatively
316 low classification accuracy, so using mixtures of images of chromosomes of various sizes is the best way
317 to create universal mitotic cell image selection models.

318 Overall, the use of models trained with images from many different species in the learning samples
319 improved the accuracy of image classifications, and the combination of only 60 images with and without
320 mitotic cells showed more than 80% accuracy in the validation (**Fig. 2**). Of these three methods validated,
321 OD showed the highest accuracy, and the options of IC were not effective (**Fig. 2** and **Fig. S2**). Considering
322 the performance per calculation time, it may be appropriate to select IC or OD depending on the situation
323 (**Table S2**). The mixed learning datasets enabled the trained models to detect those with mitotic cells from
324 samples of species not used for learning, and the OD model trained with Mix-767 showed 80-100%
325 accuracy for all types of samples (**Fig. S2**). Taken together, the results suggest that the model functions as
326 a universal mitotic cell identifier for automatically acquired cell images. In addition, these results also show

that even if this model does not work for specific samples, anyone can build their own classification models in a short time using images acquired by themselves and Create ML (**Table S3**).

To construct a semiautomatic classification system including a microscope for images containing mitotic cells, the deep learning image classifier needs to classify images taken continuously with a microscope that has automatic image capture. For this purpose, a Keyence BZ-9000 microscope was used, and the compatibility of the models generated with different microscopes from the one used for learning was confirmed. The OD model from Mix-767 was used to classify 2,458 tiled images (960 × 720 pixels each) captured by the Keyence microscope, and the OD model screened 104 images containing mitotic chromosomes with 80.6% accuracy within 2 min (**Table 1**). The accuracy of the OD model for images containing whole mitotic cells (**Fig. S3**), which is most important in cytogenetic analyses, was 90.0%. It took approximately two hours to capture 2,458 images by the microscope, but the operation time was approximately 10 min. On the other hand, it took approximately 3-4 h to manually check these areas and collect images of the mitotic cells. The total capture time was not much faster than that of the manual system, but the total operation time of the semiautomatic system was less than 20 min, which is 2.5-3.5 h less than that of manual operation. Further, the Keyence microscope used was not the latest model; the latest automatic microscope allows faster imaging such that the imaging time can be shortened. In addition,

343 the semiautomatic system allows us to obtain image datasets from broad areas of specimens, and wide-
344 range analyses can reduce artificial bias due to the selection of observation sites.

345 To obtain a more accurate model, another 150 images (Keyence-150) containing mitotic cells taken with
346 the Keyence microscope were used for object detection learning. Annotations of the cells in those images
347 were performed by manually modifying the automatic annotation by Create ML using the Mix-767 model.
348 Annotations that utilize existing models can significantly reduce the time needed for annotations. The
349 model from the combined learning dataset of Mix-767 and Keyence-150 (OD_Mix-767+Keyence-150)
350 showed 94.6% accuracy for the images containing mitotic cells (**Table 1**). The example shows that more
351 accurate models for new environments can be easily created using our models and the data obtained from
352 new environments.

353

354 **Object detection for mitotic cells in tissues**

355 As another example, detection of five phases (interphase, prophase, metaphase, anaphase and telophase) of
356 mitotic cells from confocal immunohistochemical images of *A. sativum* roots was attempted (**Fig. S4**). If
357 this detection is possible, automatic selection and classification of images containing mitotic cells from
358 images is possible. For the classification, images in PNG format of 873 interphase, 202 prophase, 119

359 metaphase, 41 anaphase and 109 telophase cells were used for learning, with 11,000 iterations. For the
360 creation of a model, the object detector took 3 h 3 min by the MacBook Air with the eGPU. A total of six
361 images, two layers each from three root sections, were manually divided such that the mitotic cells were
362 not fragmented (269 images ranging from 840 × 858 to 1,926 × 1,947 pixels), and the divided images were
363 used for validation (**Fig. 3**). The model identified the five classes of cells in the images with 68.0-92.7%
364 accuracy within 17 s (**Table 2**). In contrast, it took almost a day to manually classify these cells. The
365 accuracies are proportional to the numbers of learning data (**Fig. S5**). The accuracy was low (68.0%) for
366 anaphase, which had few training data (41 cells), but the other phases, which had 109-873 training data,
367 showed more than 81.0% accuracy. These results suggest that learning data with more than 100 cells are
368 needed to obtain more than 80% accuracy for such classifications.
369
370 **Object detection for tetrads**
371 As an example, other than dividing cells, tetrads were detected (**Fig. S6)**. Learning was performed using
372 images of 292 tetrads, and a model was created using the MacPro and Create ML with 4,000 iterations
373 within 24 min. A set of tiled images (36 × 39 × 12 z stacks = 16,848 images) was used for validation. The
374 model identified 85 out of 91 tetrads in the area from the image set within 6 min using the MacPro and

RectLabel (**Fig. S6**). The results show that the deep learning system also works well for tetrads.

Discussion

In this paper, a deep learning AI classification of microscopy images that can be easily handled by non-data scientists was attempted. As a result, even models constructed with relative few learning data were able to accurately classify dividing mitotic cells (**Fig. 2** and **Fig. S2**) and cells in tissue sections (**Fig. 3** and **Table 2**). These results indicate that non-data scientists can easily construct chromosomal image sorters for their own samples and that the constructed model can be used to semiautomate chromosomal image acquisition and selection. Deep learning-based chromosomal image classifiers already exist, but they require computing skills to handle data and tools via CLIs (LI et al. 2016; Kutsuna et al. 2012; Xiao et al. 2020; Du et al. 2011; Al-Kofahi et al. 2018; McQuin et al. 2018; Shimahara et al. 2019) or are expensive (LPIXEL's IMACEL (Shimahara et al. 2019), Nikon's NIS.ai, Olympus's TruAI, and Zeiss's ZEN Intellesis, etc.). The system applied in the present study does not require the same level of skill and can be operated by non-data scientists in the same way as GUI-based software is operated. In addition, the system requires only free tools available from Apple (Create ML), an inexpensive ($19.99 in the App Store) helper application (RectLabel), and a free file sorter (CutSort) we have developed, which allows for inexpensive

391 deep learning AI-based image classification. Recently, Apple launched new Macs with an M1 processor
392 that possesses a core for machine learning. These new Macs will enable deep learning at speeds comparable
393 to systems that combine Intel processors and eGPU without the use of an eGPU. The computing speed of
394 the M1 Macs and Intel Macs with eGPU is about one-third that of the MacPro system used in the tetrads
395 part of this study. This means that the more inexpensive system will allow the deep learning we have shown
396 in this paper. These simple and inexpensive systems may constitute a revolutionary technique for
397 cytogenetic analysis that has been performed manually.

398 In addition, the system worked well with tetrads, which are nonchromosomal objects (**Fig. S6**).
399 Basically, image classification by deep-learned AI can be done with sufficient training samples, as long as
400 the images are distinguishable to the human eye. Since Create ML is an application developed for general
401 images, there is a possibility that it can be used for scientific images other than the microscopic images
402 used here. In chromosome analysis, this system we have reported may be applicable to more complex
403 analysis such as "meiosis" and "chromosome aberration". For example, if we can use a molecular clock
404 that can determine the cell cycle in detail (Mahdessian et al. 2021), we may be able to perform more detailed
405 analysis. It would also be possible to learn about "meiosis" and "chromosome aberrations", if clear images
406 to define them were used.

Additionally, this system could be used as an advisory system as well as for object detection and classification. In this study, we annotated the objects as "mitotic cells" and "tetrads", but there are any annotations that can be used in this system. For example, the "reason for failure" is a very important point to overcome the failure for beginners in cytogenetics, but it is difficult to find without the advice of cytogeneticists. If a model is created from a data set annotated with the advice of cytogeneticists on various failure cases, the deep-learning AI may function as a "good advisor for beginners in cytogenetics". Such a system would be an effective tool for the widespread use of cytogenetic methods.

As mentioned above, we have not found any limitations in this system for image learning, detection, and classification, but the fact that it doesn't run on Windows, the most common OS in the world, may be the biggest limiting factor. In this respect, our next challenge will be to enable similar analysis using an open-source application available for Windows, since this cannot be achieved with Create ML, which is provided by Apple as a developer tool. Since this problem can be solved by obtaining an inexpensive Mac and using this system, overall, this system has the potential to be used as a "deep learning sorter that anyone can use" because it can easily build models for sorting using all kinds of biological images.

References

Abadi M, Agarwal A, Barham P, Brevdo E, Chen Z, Citro C, Corrado GS, Davis A, Dean J, Devin M, Ghemawat S, Goodfellow I, Harp A, Irving G, Isard M, Jozefowicz R, Jia Y, Kaiser L, Kudlur M, Levenberg J, Mané D, Schuster M, Monga R, Moore S, Murray D, Olah C, Shlens J, Steiner B, Sutskever I, Talwar K, Tucker P, Vanhoucke V, Vasudevan V, Viégas F, Vinyals O, Warden P, Wattenberg M, Wicke M, Yu Y, Zheng X (2015) TensorFlow: A System for Large-Scale Machine Learning. https://www.usenix.org/system/files/conference/osdi16/osdi16-abadi.pdf.

Abid F, Hamami L, Badache F, Derdour H (2017) A system on chip for automatic karyotyping system. Computers Electrical Engineering 64:1-14

Al-Kofahi Y, Zaltsman A, Graves R, Marshall W, Rusu M (2018) A deep learning-based algorithm for 2-D cell segmentation in microscopy images. BMC bioinformatics 19:365

Cremer T, Cremer C (1988) Centennial of Wilhelm Waldeyer's introduction of the term "chromosome" in 1888. Cytogenet Cell Genet 48:66-67

Du TH, Puah WC, Wasser M (2011) Cell cycle phase classification in 3D in vivo microscopy of Drosophila embryogenesis. BMC bioinformatics 12: S18

Ferguson-Smith MA, Trifonov V (2007) Mammalian karyotype evolution. Nature Reviews Genetics 8:950-962

Hernández-Mier Y, Nuño-Maganda MA, Polanco-Martagón S, García-Chávez MdR (2020) Machine Learning Classifiers Evaluation for Automatic Karyogram Generation from G-Banded Metaphase Images. Appl Sci 10 (8):2758

Jia Y, Shelhamer E, Donahue J, Karayev S, Long J, Girshick R, Guadarrama S, Darrell T (2014) Caffe: Convolutional Architecture for Fast Feature Embedding. Proceedings of the 22nd ACM international conference on Multimedia:675-678

Kato K, Matsumoto T, Koiwai A, Mizusaki S, Nishida K, Noguchi M, Tamaki E (1972) Liquid suspension culture of tobacco cells. Proc IV IFS: Ferment Technol:680-695

Kuniyoshi D, Masuda I, Kanaoka Y, Shimazaki-Kishi Y, Okamoto Y, Yasui H, Yamamoto T, Nagaki K, Hoshino Y, Koide Y, Takamure I, Kishima Y (2020) Diploid male gametes circumvent hybrid sterility between Asian and African rice species. Frontiers in Plant Science 11:579305

Kutsuna N, Higaki T, Matsunaga S, Otsuki T, Yamaguchi M, Fujii H, Hasezawa S (2012) Active learning framework with iterative clustering for bioimage classification. Nature Communications 3:1032

LI Y, Knoll JH, Wilkins RC, Flegal FN, Rogan PK (2016) Automated discrimination of dicentric and monocentric chromosomes by machine learning-based image processing. Microsc Res Tech 79:393-402

455 Mahdessian D, Cesnik AJ, Gnann C, Danielsson F, Stenström L, Arif M, Zhang C, Le T, Johansson F,
456 Shutten R, Bäckström A, Axelsson U, Thul P, Cho NH, Carja O, Uhlén M, Mardinoglu A, Stadler
457 C, Lindskog C, Ayoglu B, Leonetti MD, Pontén F, Sullivan DP, Lundberg E (2021)
458 Spatiotemporal dissection of the cell cycle with single-cell proteogenomics. Nature 590:649-654
459 Mandáková T, Lysak MA (2008) Chromosomal Phylogeny and Karyotype Evolution in x=7 Crucifer
460 Species (Brassicaceae). The Plant Cell 20:2559-2570
461 McQuin C, Goodman A, Chernyshev V, Kamentsky L, Cimini BA, Karhohs KW, Doan M, Ding L,
462 Rafelski SM, Thirstrup D, Wiegraebe W, Singh S, Becker T, Caicedo JC, Carpenter AE (2018)
463 CellProfiler 3.0: Next-generation image processing for biology. PLoS Biol 16: e2005970
464 Munot MV, Joshi MA, Sharma N (2011) Automated Karyotyping of Metaphase Cells with Touching
465 Chromosomes. International Journal of Computer Applications 29
466 Nagaki K, Cheng Z, Ouyang S, Talbert PB, Kim M, Jones KM, Henikoff S, Buell CR, Jiang J (2004)
467 Sequencing of a rice centromere uncovers active genes. Nat Genet 36 (2):138-145.
468 doi:10.1038/ng1289

Nagaki K, Terada K, Wakimoto M, Kashihara K, Murata M (2010) Centromere targeting of alien CENH3s in Arabidopsis and tobacco cells. Chromosome Res 18 (2):203-211. doi:10.1007/s10577-009-9108-0

Nagaki K, Yamamoto M, Yamaji N, Mukai Y, Murata M (2012) Chromosome dynamics visualized with an anti-centromeric histone H3 antibody in *Allium*. PLoS One 7 (12): e51315. doi:10.1371/journal.pone.0051315

O'Connor C (2008) Karyotyping for Chromosomal Abnormalities. Nature Education 1 (1):27

Pellicer J, Leitch IJ (2020) The Plant DNA C-values database (release 7.1): an updated online repository of plant genome size data for comparative studies. New Phytologist 226:301-305

Sears ER (1969) Wheat cytogenetics. Annual Review of Genetics 3:451-468

Shimahara Y, Sugawara K, Kojo KH, Kawai H, Yoshida Y, Hasezawa S, Kutsuna N (2019) IMACEL: A cloud-based bioimage analysis platform for morphological analysis and image classification. PLOS One 14 (2): e0212619

Shirley B, Li Y, Knoll JHM, Rogan PK (2017) Expedited Radiation Biodosimetry by Automated Dicentric Chromosome Identification (ADCI) and Dose Estimation. J Vis Exp 4:56245

Waldeyer W (1888) Über Karyokinese und ihre Beziehung zu den Befruchtungsvorgängen. Archiv für mikroskopische Anatomie 32:1-122

Xiao L, Luo C, Yu T, Luo Y, Wang M, Yu F, Li Y, Tian C, Qiao J (2020) DeepACEv2: Automated Chromosome Enumeration in Metaphase Cell Images Using Deep Convolutional Neural Networks. IEEE transactions on medical imaging

Figures

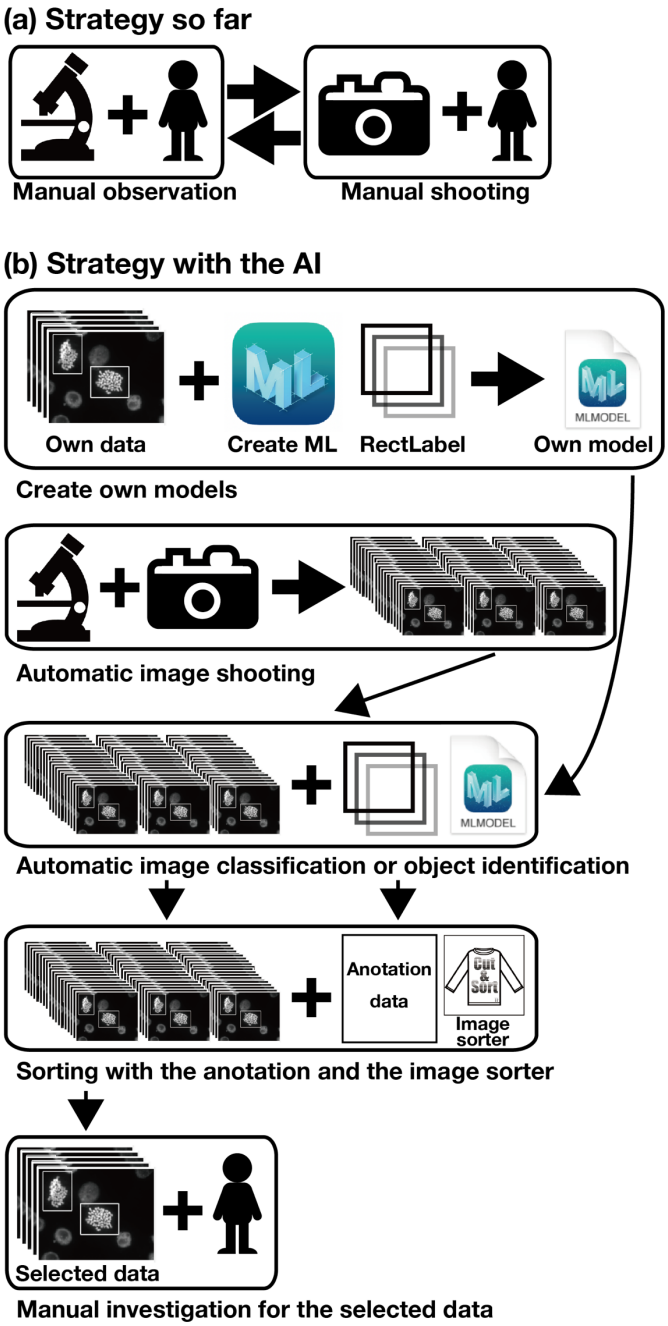

Fig. 1. Overviews of the strategies for microscopic observation so far (a) and the image acquisition and classification in this study (b).

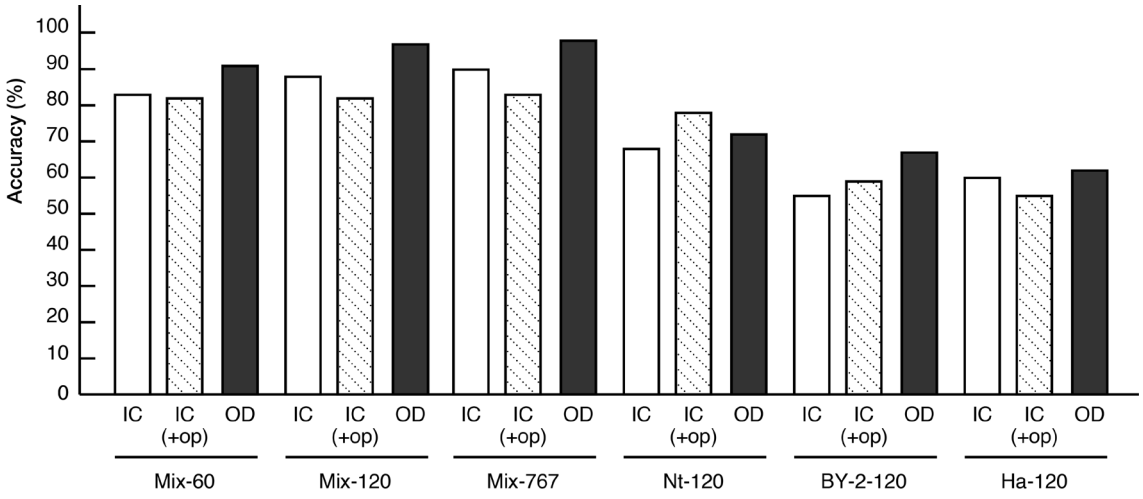

Fig. 2. Classification accuracy by models constructed with different combinations of learning data. The methods of model construction and the types of learning data are shown below the graph. IC, image classifier without options; IC (+op), image classifier with options; and OD, object detector.

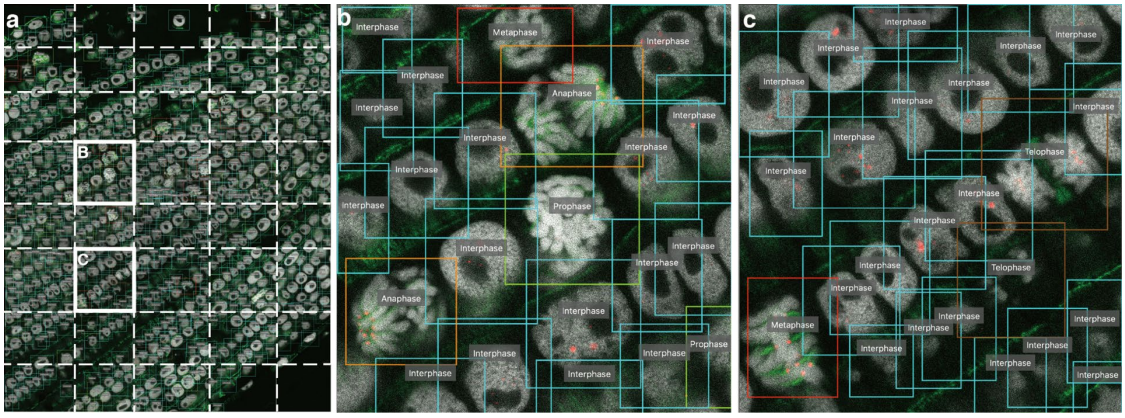

Fig. 3. Cell cycle classification for the confocal image of a root section. (a) The confocal image (7,601 × 9,415 pixels) was divided into 40 pieces at the dotted line positions, and the divided images were used for classification. The colored squares indicate mitotic cells detected by AI with the model. The white square indicates the position of the enlarged areas. (b) and (c) are the enlarged areas.

Tables

Table 1. Classification accuracy of automatically captured images.

		OD_Mix-767			OD_Mix-767 + Keyence-150		
True		Chromosomes	Others	Accuracy (%)	Chromosomes	Others	Accuracy (%)
Chromosomes	129	104	25	80.6	122	7	94.6
Chromosomes (Whole)	60	54	6	90.0	56	4	93.3
Chromosomes (Partial)	69	50	19	72.5	66	3	95.7
Others	2,329	31	2,298	98.7	39	2,290	98.3

Table 2. Cell cycle classification accuracy of the confocal images of root sections.

	True	Predicted	Accuracy (%)
Interphase	5,266	4,882	92.7
Prophase	151	127	84.1
Metaphase	58	47	81.0
Anaphase	25	17	68.0
Telophase	32	27	84.4
Total	5,532	5,100	92.2